(3D) motions at each consecutive segment of the thoracic spine have been unknown. The purpose of our study was to demonstrate *in vivo* within each intervertebral and coupled motion of the thoracic spine in trunk rotation by using the 3D imaging technique.

MATERIALS AND METHODS

Our study participants were 13 healthy male volunteers. Subjects with a history of spinal disorders, spinal surgery, lung disease, or anything that could affect spinal biomechanics were excluded. Subjects were not athletes or gymnasts. No scoliotic curve greater than 5° was found. All study protocols were approved by our institutional review board, and study participants provided written informed consent after receiving detailed information about the study.

Measurement of Intervertebral Range of Motion

Acquisition of 3D Computed Tomography

Low-dose functional computed tomographic (CT) scans were obtained for 3 positions for each subject using a commercial CT system (LightSpeed, GE Healthcare, Milwaukee, WI) with the following parameters: slice thickness, 0.625 mm; pixel size, 0.352 mm; tube rotation speed, 0.5 seconds; beam collimation, 40 mm; beam pitch, 0.9; tube current, 20 mA; and voltage, 120 kV. Subjects were placed in a neutral position that was defined as being supine on the flat CT table in a relaxed manner. The subjects' arms were held behind their heads and the pelvis was tightly fixed to the table with a belt to keep both sides of anterior-superior iliac spines parallel to the table (Figure 1). Subjects were instructed to actively rotate their shoulder girdles along with the axis of the body trunk. Rotational positions were defined as twisting the trunk at a maximum to the right and left side within a range that subjects did not feel pain or discomfort. A soft cushion device was used for the trunk to support the rotational position and for the head to be kept in the neutral position. To reduce radiation exposure, scans done in rotational positions were performed with a lower tube current, 10 mA. Total exposure was 350 dose-length products, which is less than that specified for a routine whole-spine CT by our hospital. CT data were transferred *via* digital imaging and communications in medicine network into a computer workstation, where image processing was performed using Virtual Place software (M series, Medical Imaging Laboratory, Tokyo, Japan).

Motion Analysis

The method used was fully described in our previous reports.. Contour of each vertebra was semiautomatically extracted from CT at a specific threshold. A bone window with a width of 2000 Hounsfield units and a level of 150 Hounsfield units was used for the threshold. The segmented vertebra in the neutral position was automatically superimposed on other positions by voxel-based registration. The migration was represented as a matrix. This matrix was converted into the matrix representing relative motion with respect to the inferior adjacent vertebra on the local coordinate axis. The local coordinate axis of the vertebra was defined as the right-handed orthogonal axis system in accordance with the definition provided by the Scoliosis Research Society working group (Figure 2).[12] Three-dimensional motion of each vertebra relative to the inferior adjacent vertebra was expressed in 6 degrees of freedom by Euler angles with the sequence of roll (*X*), pitch (*Y*), yaw (*Z*) in accordance with the results reported by Skalli *et al*.[13] For better understanding, relative motion of T1 vertebra with respect to L1 vertebra was also computed.

Accuracy

The accuracy of this analysis system was: 0.19° in flexion-extension, 0.13° in AR, 0.21° in lateral bending (LB), 0.13 mm in lateral translation, 0.15 mm in superoinferior translation, and 0.31 mm in anteroposterior translation, as described in detail previously.[14]

Statistical Analysis

Mean and SD for range of motion (ROM) to 1 side were computed. The thoracic spine was divided into 3 parts, upper segments: T1–T2 to T5–T6; middle segments: T6–T7 to T10–T11; and lower segments: T11–T12 to T12–L1. ARs of these segments were compared using the unpaired *t* test. The frequency of coupled LB to the same direction as AR among subjects was compared using Kruskal-Wallis rank sum test. JMP software (version 8.0.1; SAS Institute, Cary, NC) was used for statistical analysis. *P* values of less than 0.05 were considered to indicate statistical significance.

RESULTS

Data of Participants

Mean age, height, body weight, and body mass index of participants were 33.2 years (range, 30–36), 171.7 cm (range,

Figure 1. Acquisition of computed tomography. Subjects were instructed to perform maximum trunk rotation with the pelvis being fixed to the table. The arms were held behind their heads and the head was kept in the neutral position during rotation.

168–186), 70.5 kg (range, 57–91), and 23.9 (range, 20.2–30.4), respectively.

Main AR

At maximum rotation, mean ROM (± SD) of T1 with respect to L1 at 1 side was 24.9° ± 4.9° for AR, 7.6° ± 6.0° for coupled LB in the same direction as AR, and 1.8° ± 12.4° for coupled flexion.

At maximum rotation, mean ROM (± SD) of each vertebra with respect to the inferior adjacent vertebra to 1 side was 1.2° ± 0.8° at T1–T2, 1.6° ± 0.7° at T2–T3, 1.4° ± 0.9° at T3–T4, 1.6° ± 0.8° at T4–T5, 1.8° ± 0.7° at T5–T6, 1.9° ± 0.6° at T6–T7, 2.3° ± 0.7° at T7–T8, 2.5° ± 0.8° at T8–T9, 2.7° ± 0.6° at T9–T10, 2.6° ± 0.8° at T10–T11, 1.3° ± 0.7° at T11–T12, and 0.5° ± 0.4° at T12–L1 (Table 1). AR was significantly larger at middle segments (T6–T11) than at upper segments (T1–T6) and at lower segments (T11–L1) ($P < 0.01$) (Figure 3).

Coupled LB

Coupled LB with AR was observed predominantly in the same direction as AR except at T12–L1 (Figure 4). Mean ROM of coupled LB ranged from −0.1° to 2.0° (Table 1). Among subjects, the frequency of coupled LB to the same direction as AR was 92% at T1–T2, 96% at T2–T3, 92% at T3–T4, 88% at T4–T5, 88% at T5–T6, 85% at T6–T7, 85% at T7–T8, 54% at T8–T9, 54% at T9–T10, 73% at T10–T11, 65% at T11–T12, and 38% at T12–L1. There was no significant difference in the frequency of coupled LB in the same direction among subjects ($P = 0.3$).

Coupled Flexion-Extension

Coupled flexion-extension with AR was slight flexion within range of SD (Table 1).

Coupled Translation

Coupled translations were scarcely observed in lateral, anteroposterior, and superoinferior translation (Table 1).

DISCUSSION

To the best of our knowledge, this is the first *in vivo* study to measure 3D kinematics of each consecutive segment of the thoracic spine. Some *in vivo* biomechanical studies of the thoracic spine were performed in 2D methods using fluoroscopy. However, 2D analysis of spinal motions was not suitable for measurement of rotation and coupled motion, because of limitations such as potential magnification of errors, projection of translations as rotations, and masking by the shoulder girdles shadows.[15]

The current study demonstrated that AR of the thoracic spine ranged from 0.5° to 2.7° in trunk rotation. These values generally corresponded to previous studies (Table 2). Gregersen and Lucas[10] examined *in vivo* AR of random thoracic segments of 7 medical students by inserting Steinmann pins into the spinous processes. Although their results of segmental rotations were pieced by different subjects' data, total relative angle of T1 with respect to L1 was 42° and average segmental rotation divided by the number of mobile segments was 3.5°. Panjabi *et al*[8] reported that there was 1.5° to 2° of rotation in the thoracic spine by loading 5 Nm torque in 5 cadavers' study. Oxland *et al*[9] reported that rotation was 1.8° ± 0.7° at T11–T12 and 1.2° ± 0.7° at T12–L1 by loading 7.5 Nm of torque. Watkins *et al*[16] reported that total AR of T1 relative to T12 was 23.0° with intact rib cage and sternum, and their results corresponded to ours. During the *in vivo* study using a 3-space track system, Willems *et al*[7] reported rotation of the tripartite thoracic spine. The relative rotations of T1–T4, T4–T8, and T8–T12 were 13.6° ± 4.8°, 23.3° ± 5.9°, and 9.1° ± 5.2°, respectively, and thus the average segmental AR was approximately 4.5° from

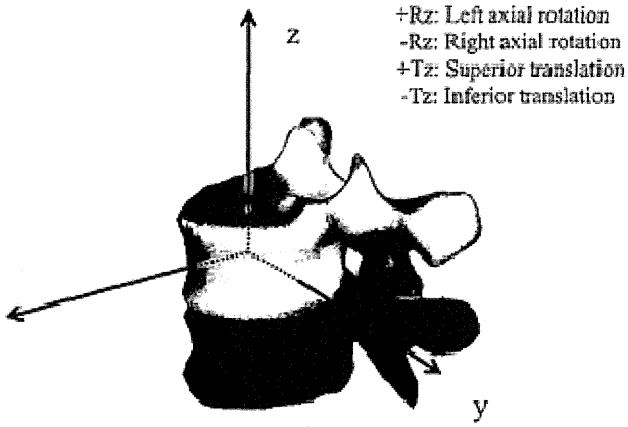

Figure 2. Orthogonal coordinate system. The origin is at the centroid of the vertebral body that is defined as half way between the centers of the 2 endplates. The local z axis passes through 2 centers of the endplates with upper being positive. The y axis is parallel to a line joining similar landmarks on the bases of the right and left pedicles with left being positive. The x axis is defined as perpendicular to z axis and y axis.

Mean (±SD) Range of Motion of the Thoracic Spine During Axial Rotation in Normal Subjects on 1 Side

Levels	Main Axial Rotation (°)	Coupled Lateral Bending (°)*	Coupled Flexion-Extension (°)†	Coupled Lateral Translation (mm)‡	Coupled SI Translation (mm)§	Coupled AP Translation (mm)¶
T1–T2	1.2 (0.8)	2.0 (1.4)	0.0 (2.1)	−0.1 (0.5)	0.1 (0.7)	0.1 (0.5)
T2–T3	1.6 (0.7)	1.8 (1.2)	−0.1 (1.5)	0.0 (0.6)	0.0 (0.6)	0.0 (0.4)
T3–T4	1.4 (0.9)	1.9 (1.5)	0.3 (1.4)	0.0 (0.5)	0.0 (0.4)	0.1 (0.4)
T4–T5	1.6 (0.8)	1.6 (1.2)	0.7 (1.0)	−0.1 (0.4)	−0.1 (0.4)	0.2 (0.3)
T5–T6	1.8 (0.7)	1.4 (1.2)	0.1 (1.0)	−0.1 (0.4)	0.0 (0.3)	0.0 (0.3)
T6–T7	1.9 (0.6)	1.1 (1.3)	0.2 (1.0)	0.0 (0.3)	−0.1 (0.3)	0.0 (0.3)
T7–T8	2.3 (0.7)	0.9 (0.8)	0.1 (0.7)	0.0 (0.3)	0.0 (0.2)	0.0 (0.2)
T8–T9	2.5 (0.8)	0.3 (0.7)	0.4 (0.5)	0.0 (0.4)	−0.1 (0.1)	0.1 (0.1)
T9–T10	2.7 (0.6)	0.1 (0.9)	0.4 (0.6)	0.0 (0.5)	0.0 (0.1)	0.1 (0.2)
T10–T11	2.6 (0.8)	0.4 (0.8)	0.5 (0.8)	0.0 (0.5)	0.0 (0.1)	0.1 (0.2)
T11–T12	1.3 (0.7)	0.6 (0.9)	1.0 (1.1)	0.0 (0.3)	0.0 (0.1)	0.3 (0.4)
T12–L1	0.5 (0.4)	−0.1 (0.9)	0.9 (0.9)	0.1 (0.4)	−0.1 (0.2)	0.3 (0.4)

*Positive means lateral bending to the same direction as axial rotation.
†Positive means flexion.
‡Positive means lateral translation to the same direction as axial rotation.
§Positive means superior translation.
¶Positive means anterior translation.
AP indicates anteroposterior; SI, superoinferior.

T1 to T4, 5.8° from T4 to T8, and 2.3° from T8 to T12. Axial rotation in our study were smaller than those in Willem's study, especially in the upper thoracic region. These differences may come from measurement errors. Skin sensors presented the possibilities of overestimating rotation angles because of displacement from spinous processes because of skin elasticity. In their study, thoracic segments for test areas were calculated solely by palpation on the back. These methodological limitations could affect results. More recently, Gercek *et al*[9] reported 1.3° of rotation at T11–T12 and 1.0° of rotations at T12–L1

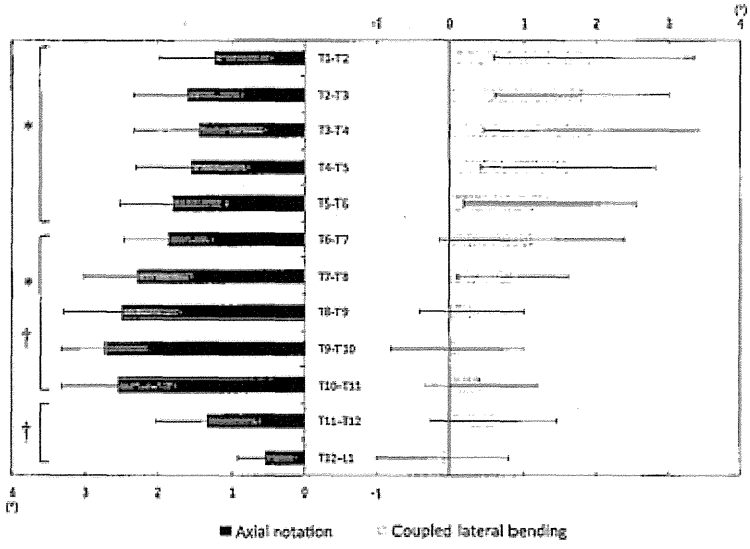

Figure 3. Mean range of motions (bar) and SD (line) of axial rotations (left) and coupled lateral bending (right) of 1 side during trunk rotations. *$P < 0.01$.

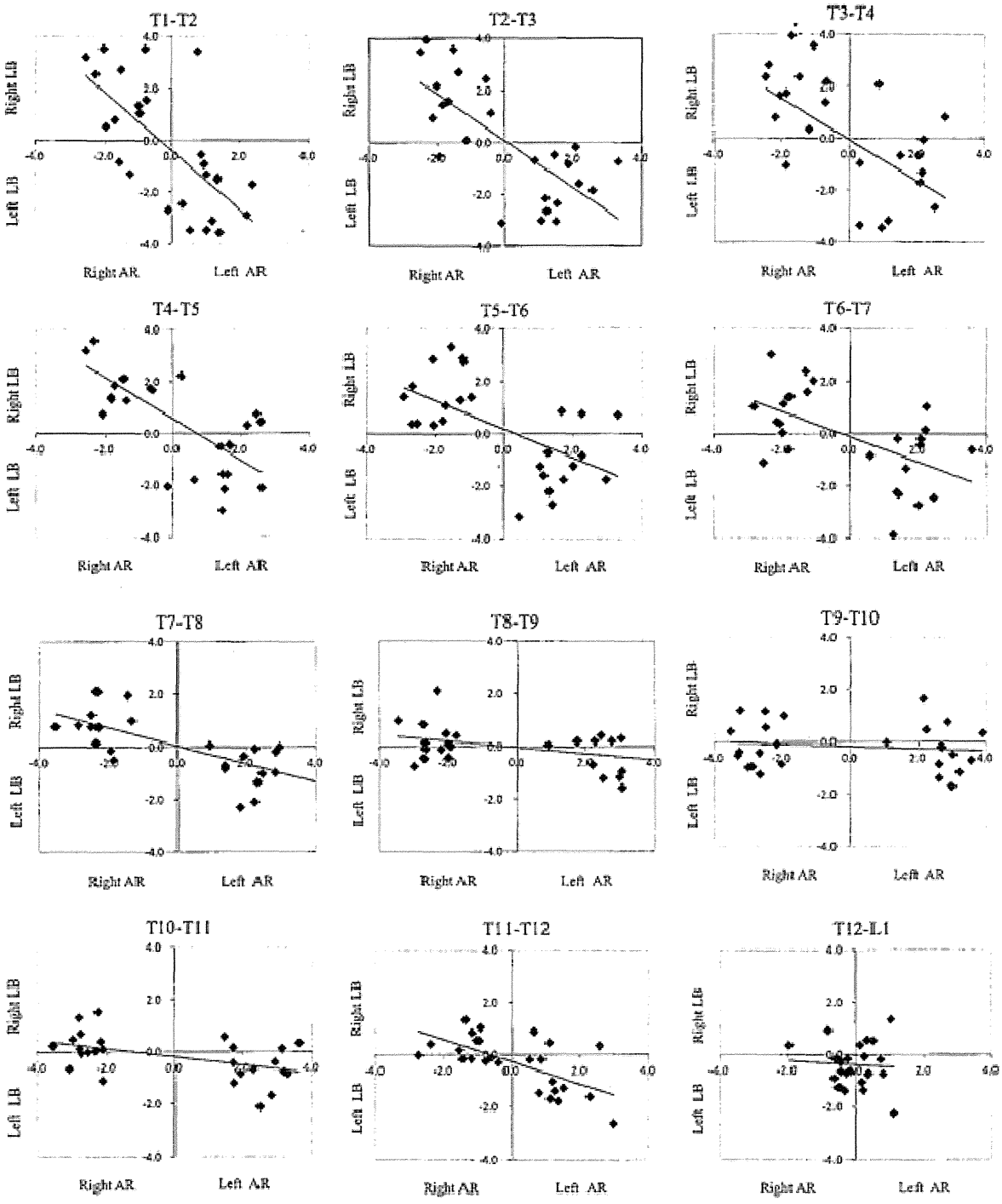

Figure 4. Relationships between axial rotation (AR) and coupled lateral bending (LB) at each spinal segment. The degree of AR was plotted on the *x* axis and the degree of coupled LB was plotted on the *y* axis. A negative slope of approximate curve meant coupled LB occurred in the same direction as AR.

Comparison of Mean (±SD) Axial Rotation (°) of the Thoracic Spine to 1 Side							
Authors	Panjabi *et al*[6]	Oxland *et al*[3]	Watkins *et al*[16]	Gregersen and Lucas[10]	Willems *et al*[7]	Gercek *et al*[9]	Present Study
Model	Cadaver	Cadaver	Cadaver	*In vivo* Pin Insertion	*In vivo* 3-Space Track System	*In vivo* Pin Insertion	*In vivo* 3D CT
Rib Cage	Only Rib Head	Only Rib Head	Intact	Intact	Intact	Intact	Intact
T1–T2	1.5–2 (NA)			16 (NA)		NA	1.2 (0.8)
T2–T3				0 (NA)	4.5* (NA)	NA	1.6 (0.8)
T3–T4				0.5 (NA)		NA	1.4 (0.9)
T4–T5				9 (NA)		NA	1.6 (0.8)
T5–T6				−5.5 (NA)		NA	1.8 (0.7)
T6–T7				6 (NA)	5.8* (NA)	NA	1.9 (0.6)
T7–T8				2.5 (NA)		NA	2.3 (0.7)
T8–T9				−2 (NA)		NA	2.5 (0.8)
T9–T10				4 (NA)	22.3* (NA)	NA	2.7 (0.6)
T10–T11				3 (NA)		NA	2.6 (0.8)
T11–T12		1.8 (0.7)		3.5 (NA)		1.3 (NA)	1.3 (0.7)
T12–L1	NA	1.2 (0.7)		NA	NA	1.0 (NA)	0.5 (0.4)
T1–T12	NA	NA	23.0 (NA)	37 (NA)		NA	24.1 (4.9)
T1–L1	NA	NA	NA	42 (NA)	NA	NA	24.9 (4.9)

*Average rotation divided by number of mobile segments.

CT indicates computed tomography; 3D, 3-dimensional; NA, (data) not available.

by *in vivo* pin insertion technique, and their results were similar to our study.

In the present study, there were significantly larger ARs observed in middle segments (T6–T7, T11–T12) than upper segments (T1–T2, T6–T7). These differences might come from the stabilization of the rib cage. The rib cage, consisting of the sternum and ribs, has a close relationship with the thoracic spine and has been regarded as a possible fourth column of the spine.[17] At typical thoracic segments, a pair of ribs articulates with the vertebra by means of 2 types of costovertebral joints. These costovertebral joints are reinforced by strong ligaments and contribute largely to stabilization of the thoracic spine. An intact rib cage was reported to account for 31% to 78% of thoracic stability.[16,18] Although the first through seventh ribs are directly connected to the sternum, the eighth through tenth ribs are indirectly connected to the sternum by means of costal cartilage. Stiffness of ribs and sternocostal and costovertebral joints at middle-lower thoracic segments was reported to be half, compared with those at upper thoracic levels.[19–20] Scapulas cover the posterior aspects of ribs 2 through 7 and may contribute to stabilization of the thoracic spine because shoulder movement has a relationship with the upper thoracic spine at these levels.[4] These anatomical characteristics of the rib cage may affect the difference of rotational motion between upper- and middle-thoracic segments.

Despite these large ARs at middle segments, ARs at T11–T12 to T12–L1 were very small. These small ARs were thought to be due to sagitalization of the facet joint articulations at thoracolumbar levels. As previously reported,[21] the orientations of facets changes dramatically for T11–L1 levels. Panjabi *et al*[22] reported that the orientation of articular facets from the sagittal plane remained approximately constant T2–T11; however, the orientation completely reversed its direction at T12–L1 levels. At these levels, the rotational motion seemed to be restricted by facet joints in the same way as by the lumbar spine.

Lovett[1] reported that concomitant coupled motions other than main motion existed during LB or rotation of the spine. It was recognized that the cervical spine had ipsilateral coupled patterns and the lumbar spine had contralateral coupled patterns except at the intersection of the atlantoaxial and lumbosacral joints.[5] However, there has been little consensus about coupled motion of the thoracic spine because of methodological difficulty in analyzing its subtle motion (Table 3).[11] Speculating from the shape of facets in the thoracic spine, coupled LB with main rotation seems to occur in the same direction, whereas in mathematical models, Schultz *et al*[5] reported that coupled LB with main rotation occurred in the same direction as rotation. Oxland *et al*[3] reported that coupled LB was 0.4° ± 0.7° in the same direction as rotation at T11–T12. White and Panjabi[5] described that coupled

Comparison of Coupled Motion With Primary Axial Rotation

Authors	Schultz *et al*[6]	Panjabi *et al*[4]	Oxland *et al*[2]	Brasiliense *et al*[13]	Gercek *et al*[9]	Willems *et al*[7]	Present Study
Model	Mathematical	Cadaver	Cadaver	Cadaver	*In vivo* Pin Insertion	*In vivo* 3-Space Track System	*In vivo* 3D CT
Lateral bending	Ipsilateral	Left	Ipsilateral	Variable	NA	Contralateral in upper, and ipsilateral in middle and lower segments	Ipsilateral in upper, and variable in middle and lower segments
Flexion-extension	NA	NA	NA	NA	Flexion	NA	Flexion

CT indicates computed tomography; 3D, 3-dimensional; NA, (data) not available.

rotation with main LB occurred in the same direction as LB at the upper thoracic segments; however, coupled rotation with main LB occurred in both directions at the middle- and lower-thoracic segments. Gregersen and Lucas[10] reported that coupled AR with main LB occurred in the same direction. If the relationship of coupled motion was reciprocal between LB and rotation, coupled LB with main rotation was speculated to occur basically in the same direction. However, in another study by Panjabi *et al*,[4] the direction of coupled LB was reported to be left in both left and right rotations. Willems *et al*[7] reported that the frequency of coupled LB in the same direction as main rotation was only 18% at T1–T4, 99% at T4–T8, and 93% at T8–T12. According to a study by Brasiliense *et al*,[13] coupled rotation with main LB occurred in the opposite direction; however, the direction of coupled LB with main rotation had variability among specimens. Gercek *et al*[9] reported that main rotation accompanied coupled flexion, but did not mention the relationship between main rotation and coupled LB. In the current study, the frequency of coupled LB in the same direction as main rotation was high at the upper segments and was accompanied by slight coupled flexion. The frequency decreased toward the lumbar spine and the coupled LB in the opposite direction predominantly occurred at the T12–L1 segment. These results suggested that coupled LB with main rotation occurred in the same direction in the upper thoracic spine in a similar pattern as the cervical spine, and likely occurred in the opposite directions at the middle and lower thoracic spine in a similar pattern as the lumbar spine (see video, Supplemental Digital Content 1, at http://links.lww.com/BRS/A683).

The current study had some limitations. First, volunteers had to be in the supine position for CT scans. Therefore, gravitational force was not considered and the ribs in contact with the CT table may have affected kinematics to some extent. Second, all subjects were male. For concern for radiation exposure, we previously used magnetic resonance imaging for analyzing kinematics of the cervical or lumbar spine. However, in the thoracic spine, it was difficult to keep the rotational position because of the longer scan time required due to the large numbers of vertebrae. The contrast images of vertebrae were less clear because of motion artifact of aorta. Thus, we decided that CT was a more suitable device for analysis of the thoracic spine. Previous reports[3–4,7,9] did not mention any large differences of kinematics between men and women. Therefore, despite these limitations, we believe that our data serve as a basis of *in vivo*, normal 3D kinematics of the thoracic spine and will be useful for better understanding of abnormal conditions of the thoracic spine.

CONCLUSION

In vivo 3D ARs and coupled motions of the consecutive thoracic spinal segments in trunk rotation were investigated. Mean AR of each segment ranged from 0.5° to 2.7°. Coupled LB was observed in the same direction as rotation in upper segments and in both directions in the middle and lower segments.

➢ Key Points

- ❑ *In vivo* 3D intervertebral ROM of the thoracic spine in trunk rotation was investigated.
- ❑ Relative rotational angle of T_1 with respect to L_1 to 1 side was 24.9° ± 4.9° in maximum trunk rotation. Segmental AR of the thoracic spine ranged from 0.5° to 2.7°. Significantly larger AR was observed at the middle segments than at the upper and lower segments.
- ❑ Coupled LB with AR was observed in the same direction as AR at the upper thoracic segments. However, in the middle- and lower-thoracic segments, coupled LB with main AR occurred both in the same and opposite directions.

Supplemental digital content is available for this article. Direct URL citations appear in the printed text and are provided in the HTML and PDF versions of this article on the journal's Web site (www.spinejournal.org).

References

1. Lovett RW. The mechanism of the normal spine and its relation to scoliosis. *Boston Medl Surg J* 1905;153:349–58.
2. Lee SM, Suk SI, Chung ER. Direct vertebral rotation: A new technique of three-dimensional deformity correction with segmental pedicle screw fixation in adolescent idiopathic scoliosis. *Spine* 2004;29:343–9.

3. Oxland TR, Lin RM, Panjabi MM. Three-dimensional mechanical properties of the thoracolumbar junction. *J Orthop Res* 1992; 10:573–80.
4. Panjabi MM, Brand RA Jr, White AA III. Mechanical properties of the human thoracic spine as shown by three-dimensional load-displacement curves. *J Bone Joint Surg Am* 1976;58:642–52.
5. White AA III, Panjabi MM. *Clinical Biomechanics of the Spine*, 2nd ed. Philadelphia PA: Lippincott Williams & Wilkins; 1990:102–4.
6. Schultz AB, Belytschko TB, Andriacchi TP, et al. Analog studies of forces in the human spine: mechanical properties and motion segment behavior. *J Biomech* 1973;6:373–83.
7. Willems JM, Jull GA, Ng JK-F. An *in vivo* study of the primary and coupled rotations of the thoracic spine. *Clin Biomech (Bristol, Avon)* 1996;11:311–6.
8. Theodoridis D, Ruston S. The effect of shoulder movements on thoracic spine 3D motion. *Clin Biomech (Bristol, Avon)* 2002;17: 418–21.
9. Gerok E, Hartmann F, Kuhn S, et al. Dynamic angular three-dimensional measurement of multisegmental thoracolumbar motion *in vivo*. *Spine (Phila Pa 1976)* 2008;33:2326–33.
10. Gregersen GG, Lucas DB. An *in vivo* study of the axial rotation of the human thoracolumbar spine. *J Bone Joint Surg Am* 1967;49:247–62.
11. Sizer PS Jr, Brismee JM, Cook C. Coupling behavior of the thoracic spine: a systematic review of the literature. *J Manipulative Physiol Ther* 2007;30:390–9.
12. Stokes IA. Three-dimensional terminology of spinal deformity. A report presented to the Scoliosis Research Society by the Scoliosis Research Society Working Group on 3-D terminology of spinal deformity. *Spine (Phila Pa 1976)* 1994;19:236–48.
13. Skalli W, Lavaste F, Descrimes JL. Quantification of three-dimensional vertebral rotations in scoliosis: what are the true values? *Spine (Phila Pa 1976) 1995;20:546–53.*
14. Fujimori T, Iwasaki M, Nagamoto Y, et al. Three-dimensional measurement of growth of ossification of the posterior longitudinal ligament. *J Neurosurg Spine* 2012;16:289–95.
15. Harrison DE, Harrison DD, Troyanovich SJ. Three-dimensional spinal coupling mechanics: Part I. A review of the literature. *J Manipulative Physiol Ther* 1998;21:101–13.
16. Watkins R IV, Watkins R III, Williams L, et al. Stability provided by the sternum and rib cage in the thoracic spine. *Spine (Phila Pa 1976) 2005;30:1283–6.*
17. Berg EE. The sternal-rib complex. A possible fourth column in thoracic spine fractures. *Spine (Phila Pa 1976) 1993;18:1916–9.*
18. Brasiliense LB, Lazaro BC, Reyes PM, et al. Biomechanical contribution of the rib cage to thoracic stability. *Spine (Phila Pa 1976)* 2011;36:E1686–93.
19. Schultz AB, Benson DR, Hirsch C. Force-deformation properties of human costo-sternal and costo-vertebral articulations. *J Biomech* 1974;7:311–8.
20. Schultz AB, Benson DR, Hirsch C. Force-deformation properties of human ribs. *J Biomech* 1974;7:303–9.
21. Malmivaara A, Videman T, Kuosma E, et al. Facet joint orientation, facet and costovertebral joint osteoarthrosis, disc degeneration, vertebral body osteophytosis, and Schmorl's nodes in the thoracolumbar junctional region of cadaveric spines. *Spine (Phila Pa 1976)* 1987;12:458–63.
22. Panjabi MM, Oxland T, Takata K, et al. Articular facets of the human spine. Quantitative three-dimensional anatomy. *Spine (Phila Pa 1976)* 1993;18:1298–310.

J Neurosurg Spine 17:74–81, 2012

Three-dimensional measurement of intervertebral range of motion in ossification of the posterior longitudinal ligament: are there mobile segments in the continuous type?

Clinical article

Takahito Fujimori, M.D.,[1] Motoki Iwasaki, M.D., Ph.D.,[1] Yukitaka Nagamoto, M.D.,[1] Masafumi Kashii, M.D., Ph.D.,[1] Takahiro Ishii, M.D., Ph.D.,[2] Hironobu Sakaura, M.D., Ph.D.,[3] Kazuomi Sugamoto, M.D., Ph.D.,[4] and Hideki Yoshikawa, M.D., Ph.D.[1]

Departments of [1]Orthopedic Surgery and [4]Orthopedic Biomaterial Science, Osaka University Graduate School of Medicine; [2]Department of Orthopedic Surgery, Kaizuka City Hospital, Osaka; and [3]Department of Orthopedic Surgery, Kansai Rosai Hospital, Hyogo, Japan

Object. In this paper, the authors' goals were to determine the extent of the effect of continuous-type ossification of the posterior longitudinal ligament (OPLL) of the cervical spine on intervertebral range of motion (ROM) and to examine the relationship between the 3D morphology of OPLL and intervertebral ROM.

Methods. The authors evaluated 5 intervertebral segments in each of 20 patients (11 men and 9 women) with continuous-type OPLL, for a total of 100 intervertebral segments, using functional CT in anteroposterior (AP) flexion and right and left axial rotation. Three-dimensional kinematics were evaluated using the voxel-based registration method. Ossification was classified on the basis of 3D kinematics and morphology.

Results. The authors found 49 ossifications that were obviously of the continuous type. They were divided into 2 types: 1) bridging (13 instances), with thick, continuous ossification of the anterior or posterior longitudinal ligament bridging intervertebral segments and with an ROM of 0.3° in AP flexion and 0.2° in rotation; and 2) nonbridging (36 instances), with a minute gap in the ossification itself or between the ossification and vertebra and with an ROM of 4.9° in AP flexion and 4.0° in rotation. There were 8 stalagmite-type ossifications in the nonbridging group that had the unique kinematics of restricted AP flexion and normal axial rotation.

Conclusions. The authors' findings indicate that most continuous-type ossifications that are categorized using the conventional radiographic classification system have mobile segments. The discrimination between bridging and nonbridging on CT scans can be a useful predictive index for dynamic factors.
(http://thejns.org/doi/abs/10.3171/2012.3.SPINE111083)

Key Words • **computed tomography** • **range of motion** • **ossification of the posterior longitudinal ligament** • **bridging-type ossification** • **in vivo 3D imaging** • **cervical spine**

Ossification of the posterior longitudinal ligament of the cervical spine is one of the causes of cervical myelopathy. Tsuyama[18] classified the types of ossification, as seen on lateral radiographs, as continuous, segmental, mixed, and localized (Fig. 1). Both static compression and dynamic factors are considered to be related to the deterioration of myelopathy.[1,4,7,8,10–15] Matsunaga et al.[11] based the importance of dynamic factors on the fact that all patients with a relatively large OPLL do not develop myelopathy. However, it is unknown to what extent dynamic factors interact with static compression in the deterioration of myelopathy. There is still controversy about how to define dynamic factors. Some researchers have reported that total ROM is significantly larger in patients with myelopathy than in those without myelopathy and that a large total ROM is thus a risk factor.[11,14] How-

Abbreviations used in this paper: AP = anteroposterior; JOA = Japanese Orthopaedic Association; OPLL = ossification of the posterior longitudinal ligament; ROM = range of motion.

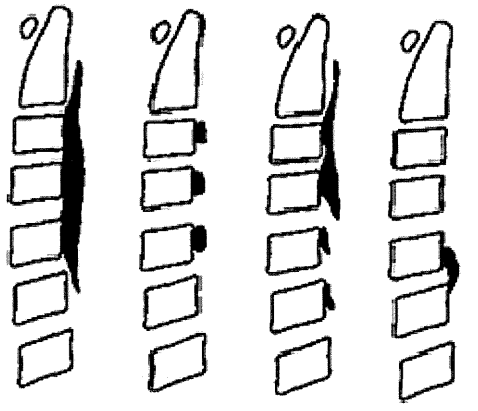

FIG. 1. The morphology of ossification based on lateral radiographs.

ever, Morio et al.[15] reported that there is no significance in total ROM between patients with myelopathy and those without it. They emphasized that the intervertebral ROM at the level responsible for myelopathy was important. Actually, in many cases, the stenosis site does not necessarily correspond to the area of abnormal mobility. Even when the stenosis site coincides with the mobile segment it is often difficult to quantify the small intervertebral ROM on functional radiography. The reliable measurable angle was approximately 3° on plain radiographs.[3,5,17]

Continuous-type OPLL was reported to have a better prognosis than mixed-type OPLL because it was erroneously believed that continuous-type OPLL is not capable of much motion.[11] However, findings on AP plain radiographs suggest that continuous-type OPLL also has some sort of motion as a whole. We conducted a study to examine the dynamic factor at each segment of continuous-type OPLL. The purpose of our study was first to measure the intervertebral ROM in continuous-type ossification and second to examine the relationship between the intervertebral ROM and the 3D morphology of ossification.

Methods

Our study participants were 20 patients with cervical OPLL who visited our facility between June 2009 and June 2010, not necessarily for their first visit. All study protocols were approved by our institution's review board. The study group included 11 men and 9 women with an average age of 64.5 years (range 40–78 years). The average JOA score was 14.7; the maximum possible score on the scale is 17. The inclusion criterion was the presence of continuous-type or mixed-type (combination of continuous-type and segmental-type) ossification, documented by plain lateral radiographs. Patients with only segmental ossification and those who had previously undergone cervical spinal surgery were excluded. Patients with moderate to severe myelopathy (JOA score < 11) were also excluded because posterior flexion could increase their myelopathy. Five intervertebral ROM measurements were obtained for each patient: C2–3, C3–4, C4–5, C5–6, and C6–7; thus, ROM was measured for a total of 100 intervertebral segments. To find obvious instances of continuous-type ossification, 4 spine surgeons evaluated radiographs of all ossifications. Only if all 4 surgeons agreed that the ossification was continuous was it included in the study.

Measurement of Intervertebral ROM

Low-dose functional CT scans were obtained for 5 positions for each patient using a commercial CT system (LightSpeed, GE Healthcare) with the following parameters: slice thickness 0.625 mm; pixel size 0.352 mm; tube rotation speed 0.5 seconds; beam collimation 40 mm; beam pitch 0.9; tube current 50 mA; voltage 120 kV. Patients were placed supine on the CT table in neutral position, at maximum AP flexion and maximum axial rotation to the left and right achievable without pain or discomfort. A supportive device was used to keep the head in anterior flexion. Patients were instructed to rotate their head as perpendicularly as possible to the axis of their body trunk, and their shoulders were horizontally fixed to the table with belts (Fig. 2). The ROM for AP flexion was calculated as the sum of the anterior flexion and the posterior flexion angle, and the ROM of axial rotation was calculated as the sum of the right rotation angle and the left rotation angle.

To reduce radiation exposure, scans done in positions other than neutral were performed with a lower tube current: 15 mA for rotation and posterior flexion and 30 mA only for anterior flexion to reduce artifact of the jawbone. Total exposure was 90 dose-length products, which is less than that specified for routine CT scanning by our hospital. The CT data were transferred via a DICOM (Digital Imaging and Communications in Medicine) network into a computer workstation, where image processing was performed using Virtual Place software (M series, Medical Imaging Laboratory). First, each vertebra was semiautomatically extracted using a process known as segmentation. A bone window with a width of 2000 HU and a level of 150 HU was used for the threshold, as has been done in earlier studies.[6] Second, the segmented vertebrae in the neutral position were superimposed on other positions using a process known as voxel-based registration. Voxel-based registration is an accurate method for determining the relative positions of 3D models at different coordinates, using a corresponding method that is based on the correlation between CT values of each voxel. This calculation is performed using software, and the relative positions are represented as a matrix. This matrix is converted to 6 df by Euler angles, with the sequence of yaw (Y), pitch (X), roll (Z), and translations, using a previously defined coordinate system.[16] As part of our study, we validated the accuracy of this method for CT scanning of the cervical spine. We performed in vitro validation of the accuracy of our experimental CT method for the cervical spine using fresh-frozen vertebrae. More than 8 tantalum beads with a radius of 1.0

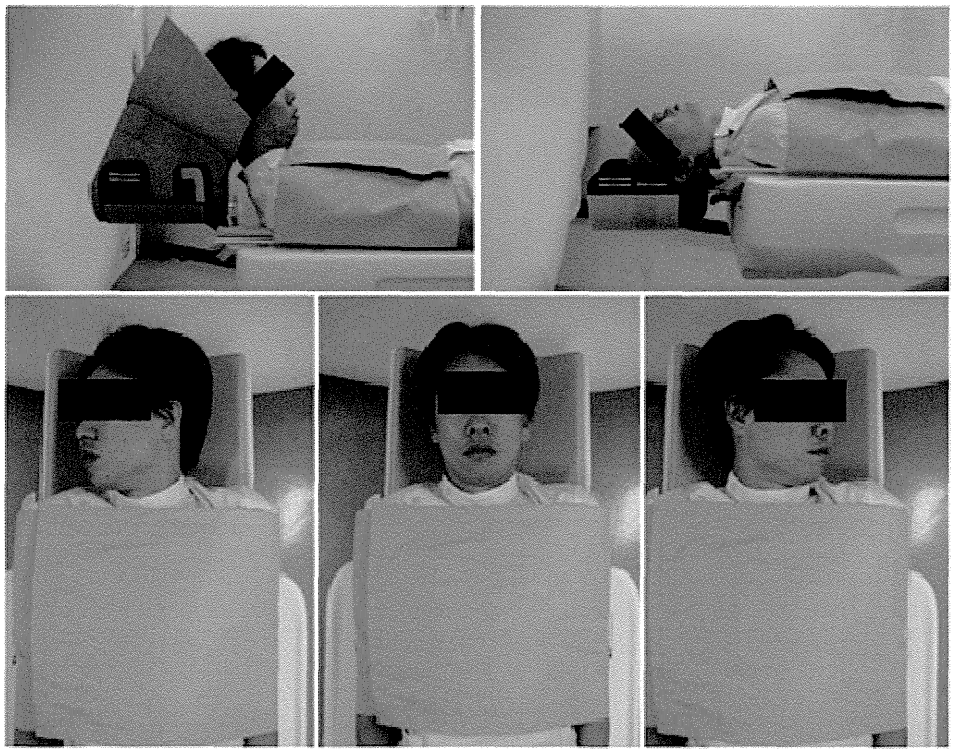

FIG. 2. Acquisition of CT scans of maximum AP flexion and maximum axial rotation. The examiner was instructed to help participants bend their necks until they could rest their chin on their chest with the use of a supportive device in anterior flexion without pain or discomfort, and to have participants rotate their head perpendicular to the axis of their body trunk.

mm were implanted in the vertebrae. Subsequently, CT scans were obtained 8 times in different positions with the same imaging parameters. Each vertebra was then superimposed by voxel-based registration. The true value of the migration was measured using marker-based registration, providing gold-standard data, and accuracy was defined as the closeness to the true value (Table 1). The root mean square distance was 0.19° in flexion-extension, 0.13° in axial rotation, 0.21° in lateral bending, 0.13 mm in lateral translation, 0.15 mm in superoinferior translation, and 0.31 mm in AP translation, demonstrating that voxel-based registration enabled far more accurate measurement than radiography.

Morphological Pattern of Ossification

The ossification pattern was classified on the basis

TABLE 1: Accuracy of voxel-based registration of the cervical spine*

Position	Rx (°)	Ry (°)	Rz (°)	Tx (mm)	Ty (mm)	Tz (mm)
1	0.26	0.08	−0.03	0.13	0.00	0.36
2	0.22	0.14	−0.11	−0.13	0.16	−0.30
3	0.06	0.08	0.29	0.10	0.03	0.41
4	−0.10	0.04	−0.28	0.02	0.07	−0.07
5	0.00	0.16	−0.09	0.13	−0.10	0.08
6	−0.21	−0.10	0.32	−0.17	0.34	0.14
7	−0.29	−0.25	−0.18	0.01	−0.05	0.58
8	0.17	0.08	−0.24	−0.19	0.12	−0.13
RMSE	0.19	0.13	0.21	0.13	0.15	0.31

* RMSE = root mean square error; Rx = flexion-extension; Ry = axial rotation; Rz = lateral bending; Tx = lateral translation; Ty = superoinferior translation; Tz = anteroposterior translation.

of 3D continuity between the ossification and the vertebra, as well as the ossification itself. All reconstructed sagittal slices with a thickness of 0.625 mm were examined on the digital viewer (AquariusNET client viewer, TeraRecon, Inc.). To perform an accurate assessment of ROM and ossification pattern, ossification of both the anterior and posterior longitudinal ligaments was covered as observation objects. The relationship between intervertebral ROM and the morphology of ossification was examined. The unpaired t-test was used for statistical analysis as appropriate with JMP software (version 8.0.1, SAS Institute). Probability values < 0.05 were considered to indicate statistical significance.

Results

Range of Motion of Intervertebral Segments

The average ROM of the 100 intervertebral segments was 7.3° in AP flexion and 3.5° in axial rotation. In those 100 intervertebral segments, continuous ossification was apparent on plain radiographs in 49 intervertebral segments. The average ROM for those segments was 3.7° in AP flexion and 3.0° in axial rotation (Table 2).

Computed Tomography Classification Based on In Vivo 3D Kinematics

Bridging and Nonbridging Ossification. We divided these 49 continuous-type ossifications into 2 groups on the basis of thin-sliced reconstructed sagittal CT scanning: bridging (Fig. 3A) with thick, continuous ossification of the anterior and/or posterior longitudinal ligament bridging intervertebral segments with bony union, and nonbridging (Fig. 3B), in which there is a minute gap in ossification itself or between the ossification and the vertebra. There were 13 bridging (27%) and 36 nonbridging (73%) ossifications. The intervertebral ROM of bridging ossifications was 0.3° in AP flexion and 0.2° in axial rotation; the respective values for nonbridging ossifications were 4.9° and 4.0° in axial rotation (Table 2). The bridging type had a significantly smaller intervertebral ROM than did the nonbridging type both in AP flexion and in axial rotation ($p < 0.001$), as shown in Video 1.

Video 1. Video clip showing 3D motion of bridging (left) and nonbridging (right) type of ossifications. Video shows that the bridging type has little motion in anteroposterior flexion and axial rotation. However, the nonbridging type has a comparatively large intervertebral range of motion. Used with permission from Takahito Fujimori. Click here to view with Media Player. Click here to view with Quicktime.

About half of the continuous ossifications were of the bridging type at the C5–6 and C6–7 levels. However, most of the continuous ossifications at the C2–3, C3–4, and C4–5 levels were of the nonbridging type. Of the 13 bridging ossifications, 10 accompanied bridging of ossification of the anterior longitudinal ligament at the same segments.

Stalagmite-Type Ossification. Among the nonbridging ossifications, 1 type had a characteristic intervertebral ROM. There was limited AP flexion and normal axial rotation in the ossifications originating from the lower vertebra and progressing continuously through and behind the upper vertebral body without contact (Fig. 3C), as shown in Videos 2 and 3.

TABLE 2: The mean intervertebral ROM of each type of ossification*

Type of Ossification	Total	Radiographically Continuous	Bridging	Nonbridging
no. of intervertebral segments	100	49	13	36
AP flexion (°)†	7.3 ± 5.6	3.7 ± 4.0	0.3 ± 0.3	4.9 ± 4.5
rotation (°)‡	3.5 ± 2.8	3.0 ± 2.9	0.2 ± 0.3	4.0 ± 2.7

* Mean values are presented as the mean ± SDs.
† Sum of anterior and posterior flexion angles.
‡ Sum of right and left rotation angles.

Video 2. Video clip showing 3D motion of the stalagmite type of ossification in anteroposterior flexion. Stalagmite-type ossifications have restricted anteroposterior flexion. Used with permission from Takahito Fujimori. Click here to view with Media Player. Click here to view with Quicktime.

Video 3. Video clip showing 3D motion of the stalagmite type of ossification in axial rotation. Stalagmite-type ossifications have normal axial rotation. Used with permission from Takahito Fujimori. Click here to view with Media Player. Click here to view with Quicktime.

We named these "stalagmite-type ossifications" because they grow slowly upward like the geologic formations. There were 8 stalagmite ossifications with an average intervertebral ROM of 1.6° in AP flexion and 4.6° in axial rotation. In comparison, the other 28 nonbridging, nonstalagmite ossifications had an average 5.9° of AP flexion and 3.9° of axial rotation. The stalagmite ossifications had significantly smaller AP flexion ($p < 0.05$) but normal axial rotation compared with the other nonbridging ossifications. All stalagmite ossifications occurred at the C2–3 or C3–4 level.

Relationship Between Neurological Symptom and Type of Ossification

We retrospectively analyzed the JOA scores of 13 patients who were monitored for more than 2 years. There were 2 patients in the bridging group whose ossifications were all bridging; the other 11 patients in the nonbridging group had at least 1 nonbridging ossification. The mean change in JOA score during the follow-up period was 0.3 points/18.5 years in the bridging group and −0.5 points/8.6 years in the nonbridging group. These results suggest that neurological function was maintained for long periods in the bridging group but that deterioration tended to occur in the nonbridging group.

Illustrative Cases

Case 1

Plain radiographs obtained in this 55-year-old woman showed apparent continuous-type ossifications; however,

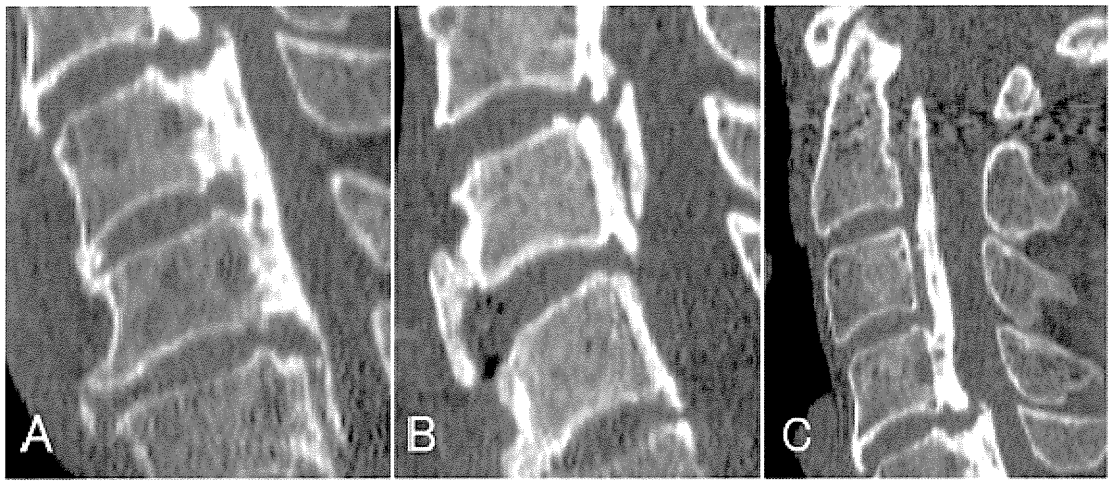

FIG. 3. Computed tomography scans showing the bridging (**A**), nonbridging (**B**), and stalagmite (**C**) types of ossification.

3D CT scanning revealed the discontinuity of ossifications in each intervertebral segment (Fig. 4). In fact, all ossifications in this patient were of the nonbridging type (Fig. 5). The intervertebral ROM in AP flexion and axial rotation was 6.5° and 10.2° at C3–C4, 7.7° and 3.4° at C4–5, 11.3° and 1.9° at C5–6, and 16.6° and 4.9° at C6–7.

Case 2

This 71-year-old man with continuous-type ossifications documented by plain radiographs had been treated conservatively with monitoring. The intervertebral ROM of AP flexion was 3.5° at C2–3, 0.9° at C3–4, 16.6° at C4–5, 13.8° at C5–6, and 13.5° at C6–7. The compensa-

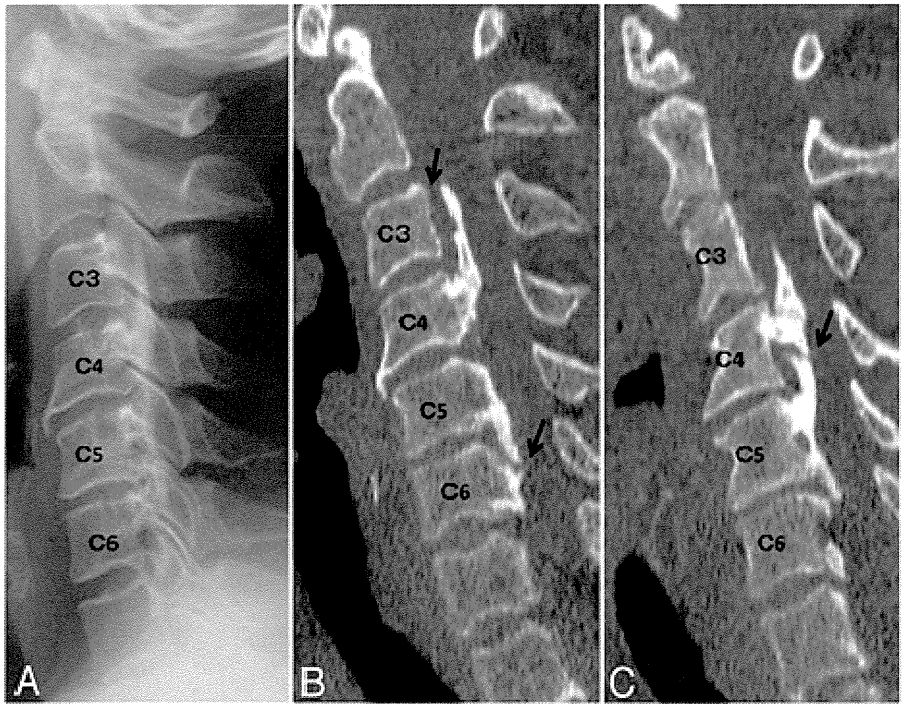

FIG. 4. Case 1. Radiograph (**A**) and CT scans (**B and C**) of ossifications. The radiograph shows a continuous-type OPLL at the C3–6 level; however, the reconstructed scans reveal the discontinuity (*arrows*) of ossifications of the nonbridging type.

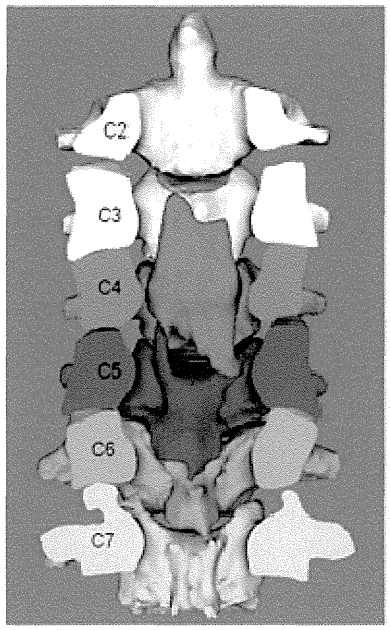

	AP flexion (°)	Rotation (°)
C2-3	8.3	2.9
C3-4	6.5	10.2
C4-5	7.7	3.4
C5-6	11.3	1.9
C6-7	16.6	4.9

FIG. 5. Case 1. Three-dimensional model, viewed from behind, of ossifications of the nonbridging type. The vertebral arches are removed for better visualization.

tory increase in ROM occurred in the adjacent intervertebral segment of C4–5. Unfortunately, the patient fell and sustained a spinal cord injury. Magnetic resonance imaging suggested that a stalagmite-type ossification hit the spinal cord like a lever, using the C4–5 mobile segment as a fulcrum point (Fig. 6).

Discussion

The 4-category classification system of the Japanese Investigation Committee on the Ossification of the Spinal Ligaments reported by Tsuyama[18] has long been the only radiographic classification system used for cervical OPLL (Fig. 1). Many studies have been performed using this classification. Matsunaga et al.[11] and Mochizuki et al.[14] reported that segmental or mixed-type ossification with a wide ROM was a risk factor for myelopathy compared with continuous-type ossification. Although the accurate quantification of intervertebral ROM has been difficult, continuous-type ossification has been considered to have fewer dynamic factors. It is true that continuous-type ossifications in our study had a comparatively small average ROM of 3.7° in AP flexion and 3.0° in axial rotation. However, the 4-category radiographic classification originally did not take dynamic factors into consideration. Actually, we found that in continuous-type ossifications, there was a marked difference in intervertebral ROM between bridging and nonbridging ossifications. These types of ossification were easily distinguishable on the basis of reconstructed sagittal CT scans. We demonstrated that on plain radiographs, 73% of continuous-type ossifications had discontinuity in some places and had 4.9° of AP flexional motion and 4.0° of rotation on average. Except for stalagmite-type ossifications, the nonbridging ossifications had as much as 5.6° of AP flexional motion. Only 27% of continuous-type ossifications corresponding to the bridging type had a little motion in the true sense. An earlier study found the prevalence of continuous-type and mixed-type ossifications on plain radiographs to be 27% and 29%, respectively;[18] however, the prevalence is different in 3D evaluation on 3D CT scans.[2,9] Chang et al.[2] reported the differences between 3D morphology on CT scans and the 4-category classification system using

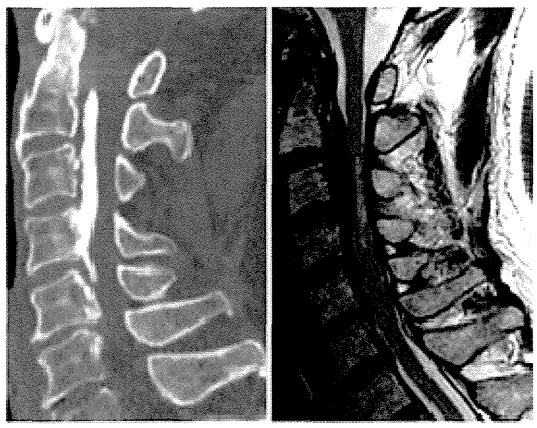

FIG. 6. Case 2. Computed tomography scan (**left**) and MRI study (**right**) of the cervical spine. The MRI study shows a T2 high-intensity area in the spinal cord at the C3–4 level.

radiographs. In their study, many continuous-type ossifications classified by radiography were reclassified as the mixed type in evaluation with CT. The kappa value of 3D CT classification was 0.86, much higher than that for radiographic classification. Kawaguchi et al.[9] also reported that 3D CT visualization provided more accurate information than radiography did. Our findings correspond with those of Chang et al. and Kawaguchi et al. Our results, which are based on 3D kinematics, could be a foundation for a new CT classification system for OPLL, one that includes dynamic factors. Further investigations of the relationship between the vertebral level responsible for myelopathy and the nonbridging-type segments will provide additional details about dynamic factors. As Fujiyoshi et al.[4] recommended, additional fusion for mobile segments in posterior decompression surgery to reduce dynamic factors may improve the prognosis. In determining the indications for additional fusion, assessment of bridging-type versus nonbridging-type ossifications can be useful.

Three-dimensional morphological evaluation also provided helpful anatomical information. Stalagmite-type ossifications had continuity of the ossification itself but were separated from the posterior wall of the upper vertebra. The long ossification originating from the lower vertebra extended behind throughout the length of the upper vertebra and was thought to block the upper vertebra so that it could not shift posteriorly. Therefore, the intervertebral segment of stalagmite-type ossifications had normal axial rotation but restricted AP flexion. We speculate that the reason this type of ossification existed only in the upper cervical spine derived from the anatomical morphology of the posterior longitudinal ligament. In the transitional process of the posterior longitudinal ligament to the tectorial membrane, the posterior longitudinal ligament may separate from the posterior wall of the vertebra by covering the transverse ligament behind the C-2 dens. Therefore, the ossification hardly attaches to the C-2 vertebra even when the posterior ligament ossifies. Interestingly, the original illustration of the radiographic classification system that appeared in the report by Tsuyama[18] observantly depicted the separation from the posterior wall of C-2 that is characteristic of continuous-type ossification (Fig. 1), although nothing was explained in the figure legends in that report.

Conclusions

Although ossification may seem to be of the continuous type on plain radiographs, the type actually comprises 2 kinds of ossification: 1) the bridging type, which has virtually no motion clinically; and 2) the nonbridging type, which has an average of 4.9° of AP flexion and 4.0° of rotation. The discrimination between bridging and nonbridging ossification on sagittal CT scans is a practical index for the existence of dynamic factors.

Disclosure

This work was supported by a grant-in-aid from the Investigation Committee on Ossification of the Spinal Ligaments, Japanese Ministry of Public Health, Labor, and Welfare, and a grant-in-aid for Scientific Research C (KAKENHI:22591632) from the Japan Society for the Promotion of Science. No benefits in any form have been or will be received from a commercial party related directly or indirectly to the subject of this manuscript. Our institution's review board approved the study reported in this manuscript.

Author contributions to the study and manuscript preparation include the following. Conception and design: Fujimori, Iwasaki. Acquisition of data: Fujimori. Analysis and interpretation of data: Fujimori, Nagamoto. Drafting the article: Fujimori. Critically revising the article: all authors. Reviewed submitted version of manuscript: all authors. Approved the final version of the manuscript on behalf of all authors: Fujimori. Statistical analysis: Fujimori. Administrative/technical/material support: Iwasaki, Sugamoto, Yoshikawa. Study supervision: Iwasaki.

Acknowledgments

The authors thank the Investigation Committee on the Ossification of the Spinal Ligaments of the Japanese Ministry of Health, Labor, and Welfare; and Scientific Research (C) from the Ministry of Education, Culture, Sports, Science, and Technology. Katharine O'Moore-Klopf, ELS (East Setauket, NY), provided professional English-language editing of this article.

References

1. Azuma Y, Kato Y, Taguchi T: Etiology of cervical myelopathy induced by ossification of the posterior longitudinal ligament: determining the responsible level of OPLL myelopathy by correlating static compression and dynamic factors. **J Spinal Disord Tech 23:**166–169, 2010
2. Chang H, Kong CG, Won HY, Kim JH, Park JB: Inter- and intra-observer variability of a cervical OPLL classification using reconstructed CT images. **Clin Orthop Surg 2:**8–12, 2010
3. Côté P, Cassidy JD, Yong-Hing K, Sibley J, Loewy J: Apophysial joint degeneration, disc degeneration, and sagittal curve of the cervical spine. Can they be measured reliably on radiographs? **Spine (Phila Pa 1976) 22:**859–864, 1997
4. Fujiyoshi T, Yamazaki M, Okawa A, Kawabe J, Hayashi K, Endo T, et al: Static versus dynamic factors for the development of myelopathy in patients with cervical ossification of the posterior longitudinal ligament. **J Clin Neurosci 17:**320–324, 2010
5. Harrison DE, Harrison DD, Cailliet R, Troyanovich SJ, Janik TJ, Holland B: Cobb method or Harrison posterior tangent method: which to choose for lateral cervical radiographic analysis. **Spine (Phila Pa 1976) 25:**2072–2078, 2000
6. Inoue S, Goto S, Nagase J, Tanaka Y: Investigation of window width and window level of computed tomography for OPLL, in **Annual Report of Taskforce of Research for Ossification of the Spinal Ligaments.** Tokyo: Japanese Ministry of Public health and Welfare, Vol 58, 1984, pp 237–239
7. Iwasaki M, Okuda S, Miyauchi A, Sakaura H, Mukai Y, Yonenobu K, et al: Surgical strategy for cervical myelopathy due to ossification of the posterior longitudinal ligament: Part 1: Clinical results and limitations of laminoplasty. **Spine (Phila Pa 1976) 32:**647–653, 2007
8. Iwasaki M, Okuda S, Miyauchi A, Sakaura H, Mukai Y, Yonenobu K, et al: Surgical strategy for cervical myelopathy due to ossification of the posterior longitudinal ligament. Part 2: Advantages of anterior decompression and fusion over laminoplasty. **Spine (Phila Pa 1976) 32:**654–660, 2007
9. Kawaguchi Y, Urushisaki A, Seki S, Hori T, Asanuma Y, Kimura T: Evaluation of ossification of the posterior longitudinal ligament by three-dimensional computed tomography and magnetic resonance imaging. **Spine J 11:**927–932, 2011

10. Liu T, Xu W, Cheng T, Yang HL: Anterior versus posterior surgery for multilevel cervical myelopathy, which one is better? A systematic review. **Eur Spine J 20:**224–235, 2011
11. Matsunaga S, Kukita M, Hayashi K, Shinkura R, Koriyama C, Sakou T, et al: Pathogenesis of myelopathy in patients with ossification of the posterior longitudinal ligament. **J Neurosurg 96 (2 Suppl):**168–172, 2002
12. Matsunaga S, Nakamura K, Seichi A, Yukoyama T, Toh S, Ichimura S, et al: Radiographic predictors for the development of myelopathy in patients with ossification of the posterior longitudinal ligament: a multicenter cohort study. **Spine (Phila Pa 1976) 33:**2648–2650, 2008
13. Matsunaga S, Sakou T, Taketomi E, Nakanisi K: Effects of strain distribution in the intervertebral discs on the progression of ossification of the posterior longitudinal ligaments. **Spine (Phila Pa 1976) 21:**184–189, 1996
14. Mochizuki M, Aiba A, Hashimoto M, Fujiyoshi T, Yamazaki M: Cervical myelopathy in patients with ossification of the posterior longitudinal ligament. Clinical article. **J Neurosurg Spine 10:**122–128, 2009
15. Morio Y, Nagashima H, Teshima R, Nawata K: Radiological pathogenesis of cervical myelopathy in 60 consecutive patients with cervical ossification of the posterior longitudinal ligament. **Spinal Cord 37:**853–857, 1999
16. Nagamoto Y, Ishii T, Sakaura H, Iwasaki M, Moritomo H, Kashii M, et al: In vivo three-dimensional kinematics of the cervical spine during head rotation in patients with cervical spondylosis. **Spine (Phila Pa 1976) 36:**778–783, 2011
17. Polly DW Jr, Kilkelly FX, McHale KA, Asplund LM, Mulligan M, Chang AS: Measurement of lumbar lordosis. Evaluation of intraobserver, interobserver, and technique variability. **Spine (Phila Pa 1976) 21:**1530–1536, 1996
18. Tsuyama N: Ossification of the posterior longitudinal ligament of the spine. **Clin Orthop Relat Res (184):**71–84, 1984

Manuscript submitted December 21, 2011.
Accepted March 12, 2012.
Please include this information when citing this paper: published online April 27, 2012; DOI: 10.3171/2012.3.SPINE11083.

Supplemental online information:

Video 1: http://mfile.akamai.com/21490/wmv/digitalwbc.download.akamai.com/21492/wm.digitalsource-na-regional/spine11-1083_video_1.asx (Media Player).
http://mfile.akamai.com/21488/mov/digitalwbc.download.akamai.com/21492/qt.digitalsource-global/spine11-1083_video_1.mov (Quicktime).
Video 2: http://mfile.akamai.com/21490/wmv/digitalwbc.download.akamai.com/21492/wm.digitalsource-na-regional/spine11-1083_video_2.asx (Media Player).
http://mfile.akamai.com/21488/mov/digitalwbc.download.akamai.com/21492/qt.digitalsource-global/spine11-1083_video_2.mov (Quicktime).
Video 3: http://mfile.akamai.com/21490/wmv/digitalwbc.download.akamai.com/21492/wm.digitalsource-na-regional/spine11-1083_video_3.asx (Media Player).
http://mfile.akamai.com/21488/mov/digitalwbc.download.akamai.com/21492/qt.digitalsource-global/spine11-1083_video_3.mov (Quicktime).

Address correspondence to: Takahito Fujimori, M.D., Department of Orthopedic Surgery, Osaka University Graduate School of Medicine, 2-2 Yamadaoka, Suita, Osaka 565-0871, Japan. email: takahito-f@hotmail.co.jp.